Characterizing nanoimprint profile shape and polymer flow behavior using visible light angular scatterometry

Rayan M. Al-Assaad, Suresh Regonda, and Li Tao
Department of Electrical Engineering, University of Texas at Dallas, Richardson, Texas 75083

Stella W. Pang
Department of Electrical Engineering and Computer Science, University of Michigan, Ann Arbor, Michigan 48105

Wenchuang (Walter) Hu[a)]
Department of Electrical Engineering, University of Texas at Dallas, Richardson, Texas 75083

(Received 10 June 2007; accepted 24 September 2007; published 10 December 2007)

The profile shape and the flow behavior of polymer nanoscale gratings made by a thermal nanoimprint process are precisely examined using visible light angular scatterometry. Nanoimprinted poly(methyl methacrylate) (PMMA) lines with 60–800 nm width, 100–200 nm height, and varied residual thicknesses of 70–400 nm have been investigated using this optical approach, and insightful observations are made regarding residual stress buildup during thermal nanoimprint. In addition, a nonlinear profile model has been developed for scatterometry to monitor the "melting" behavior of PMMA gratings under annealing around its glass transition temperature. The polymer nanostructures were found to relax primarily at high stress regions. © *2007 American Vacuum Society.* [DOI: 10.1116/1.2800327]

I. INTRODUCTION

The ability to fabricate polymer nanostructures is vital not only for the evolution of integrated circuit (IC) technology but for many emerging optical, electromechanical, and biomedical nanotechnologies as well. Nanoimprint lithography[1,2] excels as a cost-effective manufacturing technique with sub-10-nm resolution[3,4] and has been considered by the semiconductor industry since 2004 as a candidate for next generation lithography technology.[5]

With increasing downscaling in patterning nanostructures, metrology is also becoming more challenging. Moreover, in order to control nanoimprint processes to achieve good fidelity, the understanding of polymer flow behavior during the nanoimprint process is critical. For this purpose, not only line dimensions and residual thickness but also polymer stresses and stability need to be quantified. These needs are beyond the capability of current metrology tools such as scanning electron microscopy (SEM), atomic force microscopy (AFM), and conventional scatterometry.[6] Recently, highly sensitive techniques based on small angle x-ray scattering[7,8] (CD-SAXS) and specular x-ray reflectivity[9] (SXR) from periodic patterns have been developed to characterize polymeric grating dimensions and to monitor relaxation of polymer nanostructures during thermal annealing.[10] However, widespread use of CD-SAXS may be limited by the high cost of strong x-ray sources as well as the effect of x-ray radiation in functional polymers. In general, optical metrology such as scatterometry is ideal to characterize polymer nanostructures because of its low cost, fast speed, and minimal sample damage. However, the functionality is very limited for nanoimprinted structures to date. Lately, a spectral scatterometry has been applied to measure the residual thickness and line dimensions for nanoimprinted polymer structures.[11] The employed rectangular model, however, is limited in yielding accurate results for line profiles with sidewall slopes or curved sidewall shapes.

Here, a visible light angular scatterometry (VLAS) tool and modeling algorithms with new functionalities were built to characterize the dimensions, profile shape, and residual thickness of the imprinted polymer nanostructures. The first aim is to demonstrate the feasibility and accuracy of this noninvasive, reliable, and low-cost metrology tool for characterizing nanostructures. The second aim is to apply this metrology to study the effect of polymer thickness on the polymer flow behavior, stability, relaxation upon heating, and internal stress in the nanoimprinted nanostructures. Previous simulation and experimental work has shown that polymer deformation is strongly related to the mold geometry and dimensions, polymer thickness, and polymer capillary and viscous flow behaviors.[12–15] Here, the accurate characterization of polymer nanostructures using the VLAS leads to some experimental observations of the effect of polymer thickness on the flow behavior during the nanoimprint process, the relationship of residual thickness to the polymer stress, and stability or relaxation behavior of polymer nanostructures, which are helpful to understand and optimize the nanoimprint process.

II. EXPERIMENT

A variable angle scatterometer with a red laser HeNe source was built based on a 2-θ configuration, as described in detail in the previous work.[16] In this angular configuration shown in Fig. 1, measurements are made by varying the angle of incidence θ_{inc} from 20° to 80° and recording the

[a)]Electronic mail: walter.hu@utdallas.edu

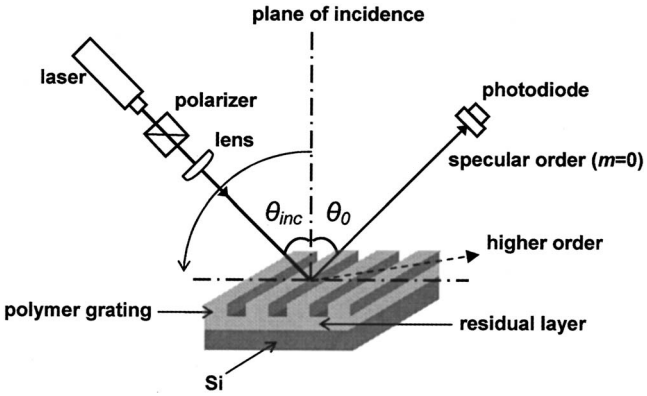

FIG. 1. Schematics of a 2-θ angular scatterometry configuration used in VLAS.

reflected zeroth order power at each angle. Use of a red wavelength (633 nm) for the measurements was also examined, and it was found to possess sufficient sensitivity (above the measurement noise level) in the VLAS technique to resolve nanoimprint line critical dimensions as small as 20 nm. Details of the sensitivity analysis are discussed elsewhere.[16] A linear regression algorithm[17] is used to process the angular reflectance data and retrieve the structure dimensions by fitting the measurements to the rigorous coupled wave approximation (RCWA) model.[18] A trapezoidal model is chosen for the line profile, characterized with the following parameters: height, width, sidewall slope angle, and additionally residual layer thickness. Furthermore, a profile model with multiple rectangular layers is used to represent line profiles with curved or nonlinear sidewalls. Since stress may be built up during thermal nanoimprint, the refractive index of polymer gratings may change. This issue is considered in the model construction and the refractive index is first searched for the best fit to scatterometry measurements.

As measured by special ellipsometry and profilometry, 950 000 molecular weight polymethylmethacrylate (PMMA) with varying thicknesses of 120, 220, 400, and 620 nm was spincoated onto Si substrates. The samples were then baked on a hot plate at 170 °C for 5–30 min depending on the PMMA thickness. Si molds that consist of micro- and nanoscale line and space gratings were used to generate 1 μm and sub-100-nm gratings in the PMMA films using an Obducat 2.5 nanoimprinter operating at a temperature of 165–180 °C and a pressure of 6 MPa for 10–15 min. The mold was released from the PMMA substrates after cooling to 70 °C, which is significantly below the glass transition temperature (T_g) of PMMA. The micro- and nanoscale PMMA gratings cover areas of 5×5 and 2×4 mm^2, respectively. After measurements with scatterometry, a thin layer of AuPd (60:40) was sputtered on the PMMA structures, and their cross-sectional profiles were evaluated in a SEM and compared to the scatterometry results. In order to prevent PMMA shrinkage and deformation during the SEM imaging, rapid scan speed, low e-beam energy (2 keV), and small beam current (<30 pA) were used: hence the image quality is sacrificed to preserve the geometry of the PMMA structures.

III. RESULTS AND DISCUSSION

A. Characterization of line profile and residual thickness

The VLAS measurement data and results using the trapezoidal model for the PMMA gratings with four different initial film thicknesses, h_i=120, 220, 400, 620 nm, are shown in Fig. 2(a). Table I lists the resolved pattern height (h_p), width (w_p), slope angle (θ), residual thickness (h_r), optimized optical index (n) in the theoretical modeling, and the fit errors between the model and the experiments. The fitting of the modeled reflectance curves is very close to the experimental data, indicating high measurement accuracy. Note that the VLAS measurements of the nanostructures are averaged over a sample area of 1 mm^2, which may not represent exactly the nanostructure geometry at one particular location captured by the SEM image. Therefore, some degree of variation between scatterometry and SEM results is typically expected. The fit errors are observed to increase monotonically as the initial PMMA thickness h_i increases. For the 620 nm sample, the fit error increases sharply, which is attributed to a larger nonuniformity in the residual layer due to the mold bending in comparison to the other samples. The high imprint pressure on a mold with "nonoptimal" geometry causes the mold bending/deformation and consequently the formation of a nonuniform residue layer.[19,20] It is verified from the SEM evaluation that the residual thickness at the center of the patterned area is almost 100 nm less than the edge of the area for the 620 nm sample. The line profile and residual thickness as resolved from VLAS measurements, for the two samples with initial 120 and 620 nm PMMA thicknesses, are scaled in the SEM cross-sectional images shown in Fig. 2(b). Good agreement of the measurements with the SEM images is observed.

For the 220 nm PMMA sample, an unusual increase in modeled PMMA index from 1.49 to 2.12 was found necessary in order to achieve a good fit to the data, as shown in Table I. In addition, the smallest linewidth (~60 nm) was found in this sample. This unusually high index value determined by the physical modeling for this particular PMMA thickness may not represent its actual index value, but signifies nonetheless a change in the index after imprinting. Repeated experiments for various samples with the same conditions revealed similar increase in the optical index value. This leads us to believe that the change in the index may be related to significantly high stress buildup in the PMMA nanostructures and residual layers during the nanoimprint process under such PMMA thickness conditions. Most previous studies of polymer deformation during nanoimprint process were based on a volume conservation rule, where the polymer is assumed as a viscous and incompressible material.[13–15] For our experiments, the ratio of cavity width to spacing of the mold ($w:s$) is 2:5, and therefore excessive polymer needs to be relocated during the nanoimprint processes. The total changes in the polymer cross-sectional areas after imprinting (ΔA) are calculated based on the measured dimensions and are listed in Table I. The reduction of

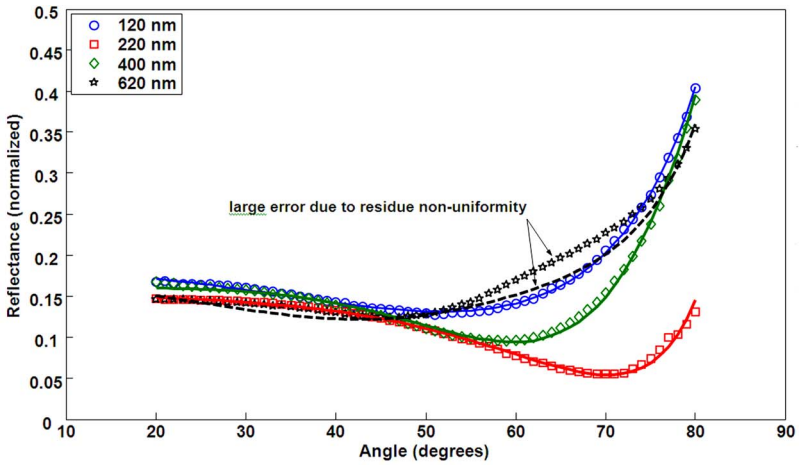

(a)

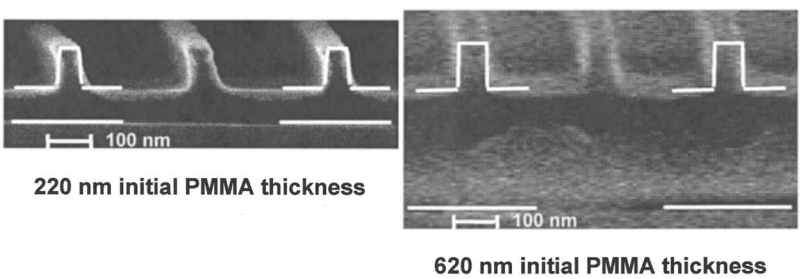

(b)

FIG. 2. (a) The angular scatterometry measurements and modeling results for the PMMA gratings with four different initial PMMA thicknesses of 120, 220, 400, and 620 nm. (b) The scatterometry resolved grating profiles are scaled to the cross-sectional SEM images for two cases: 120 and 620 nm initial PMMA thicknesses.

the cross-sectional area is found to be significant and increases with the increasing PMMA thickness. This indicates that for the 220–620 nm PMMA samples, either a significant amount of polymer is pushed outside of the pattern toward sample edges resulting in nonuniform residual layer or the polymer is compressed resulting in high stress and higher refractive index.

In order to interpret these observations, a polymer flow model is proposed in Fig. 3(a). A mold with concave width (w), spacing width (s), and a pitch $p=w+s$ is pressed into a polymer film with initial thickness h_i under a uniform pressure, resulting simultaneously in an upward flow of the polymer toward the cavities in the mold and a longitudinal flow across the pattern area. Previous theoretical studies show that the mold spacing width to polymer thickness ratio (s/h_r) determines the vertically or laterally dominant deformations.[13,14] The geometry ratio significantly affects the stress distribution in the polymer structures and the residual layer. Here, the PMMA structures are simply divided into two layers, as shown in Fig. 3(a). The top layer [shadowed area in Fig. 3(a)] consists of the polymer filling the cavity and the top residual layer, which is highly stressed. The remaining residual layer is treated as a less stressed layer. In order to find experimental evidence of this stress assumption in the model, a nanoimprint experiment was performed using partially cured SU-8 resist because of its rigidity. The SU-8 rippling under the nanoimprint pressure was observed during the polymer flow to fill the mold, as shown in Fig. 3(b).

TABLE I. Resolved line height, width, slope, and residual thickness for nanoimprinted PMMA gratings with various initial thicknesses. The optimized optical index, the fit errors between experiment and theoretical modeling, the total change in cross sectional area (ΔA) before and after imprinting, and the ratio of the mold spacing width to the residual thickness are also shown.

Initial thickness h_i (nm)	Height h_p (nm)	Width w_p (nm)	Slope θ (deg)	Residual h_r (nm)	Index n	Fit error	ΔA (nm^2)	s/h_r ratio
120	160	109	7	74	1.49	2×10^{-4}	−379	3.4
220	109	60	7	114	2.12	5×10^{-4}	30 691	2.2
400	144	78	15	330	1.49	8×10^{-4}	8 762	0.8
620	126	81	1	350	1.49	1.4×10^{-2}	88 067	0.7

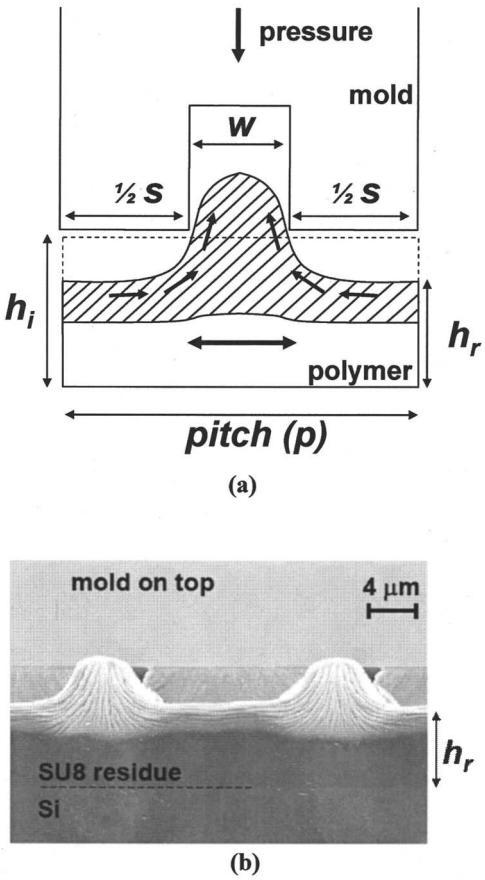

FIG. 3. (a) A two-layer polymer flow model for a concave mold with the w/s ratio less than 0.5. (b) A cross-sectional SEM image of a 20 μm pitch SU-8 gratings on Si. The SU-8 was partially cured with UV light on purpose before the nanoimprint so that the "rippling" pattern is observed after nanoimprint to visualize the stress distribution in the polymer structures.

Interestingly, the SU-8 patterns show two layers with different electron contrasts in SEM, which matches well to the two-layer model we proposed in Fig. 3(a). The SU-8 ripples visualized the polymer flow and the polymer stress built up during the nanoimprint process. The high stress is located at pattern corners with high curvatures and also at the top portion of the residual layer. The s/h_r ratio of this SU-8 sample is about 1.75, which indicates that the polymer flow is dominated by the squeeze flow mode.[13,14]

Based on this simple model and considering the 120 nm PMMA sample, the total reduction of the cross-sectional area ΔA is negative and small, which means that the amount of polymer available matches the needs of cavity filling. The polymer flows smoothly toward the mold cavities, followed by thermal relaxation in the cavity. As a result, cavity filling was more complete, with a larger height of 160 nm and width of 109 nm, close to the mold dimensions (depth of 170 nm and width of 110 nm), as well as a typical index of 1.49, in comparison to the other samples. For the 220 nm PMMA sample on the other hand, ΔA is significant and a large increase in the optical index is found. The line height and width appear to be significantly smaller those of the other samples. This can be explained as follows. The s/h_r ratio of this sample is about 2.2 and therefore the polymer flow is mainly squeeze flow. Considering the excessive amount of polymer available to fill the mold, the slow squeeze flow will induce high stress in the polymer and possibly compress it as well, which then slows down the mold filling process, resulting in incomplete filling of the mold cavities. The drastic change in the index for the scatterometry modeling likely reflects qualitatively the high stresses in the 220 nm sample. This high stress is likely the reason for the fast structural relaxation upon heating, as discussed in the next section. For the 400 and 620 nm samples, although there is excessive amount of polymer to fill the mold, the thick residual layer allows the fast shear flow to fill the mold and at the same time flow outside the pattern areas. Therefore, both samples reveal typical optical index and better mold filling than the 220 nm sample. However, for the thick PMMA samples, the mold bending and polymer shear flow result in a nonuniform residue layer, which is a serious drawback for pattern transfer.[20] Based on these observations, polymer thickness should be chosen to supply an appropriate, not less or excessive, amount for the specific mold dimensions to achieve good transfer fidelity and alleviate polymer stress and residue nonuniformity.

B. Characterization of relaxation behavior of polymer nanostructures

The VLAS technique was used to further investigate polymer flow behavior upon thermal annealing for both micro- and nanoscale PMMA structures. In order to precisely represent the curved line profiles, a new VLAS model is constructed by dividing the line profile into a stack of 5–20 rectangular layers. The widths of the stacked layers are varied from line top to bottom according to a cubic function to achieve the best fit to the scatterometry measurements.

As shown in the previous section, the 220 nm thick PMMA samples with 365 nm pitch gratings display a high optical index and poor mold filling, possibly indicating high stress in the polymer. The same sample was investigated under this thermal annealing study, with the aim of finding more evidence of the stress. In addition, another 870 nm wide, 2 μm pitch, 215 nm high PMMA grating (initial thickness of 455 nm) was used in the study for comparison. Both the 365 nm pitch and the 2 μm pitch samples were heated at 100 °C (around the T_g of PMMA) for 2 and 4 min respectively. The VLAS measurements were performed before and after the heating process and the data are shown in Fig. 4(a) for the two samples. A significant increase in the reflectance curve is noticed at the small angles for the large pitch sample, and also at the large angles for the small pitch sample. This increase in measurement values at the two edges of the angular spectrum corresponds to a transition in the reflectance behavior from a grating surface with some diffraction characteristics toward a flatter surface with more Fresnel-like characteristics. The nonlinear profile model used in this study shows a significantly better fit in the line sidewall shapes which is confirmed in the SEM pictures as well [Fig. 4(b)]. A similar trend in both examined samples is ob-

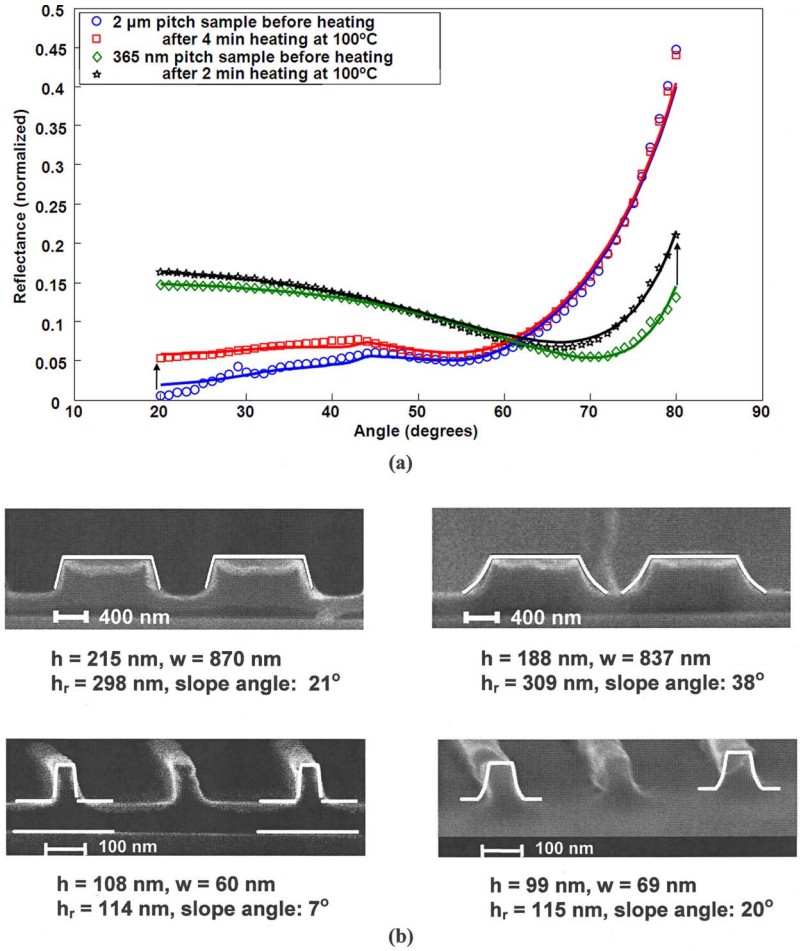

FIG. 4. (a) The scatterometry measurements and modeling results for both 2 μm and 365 nm pitch PMMA gratings prior and after heating at 100 °C. (b) The grating profiles resolved by the nonlinear sidewall model in the scatterometry are scaled to the cross-sectional SEM images.

served regarding the changes in the profile during thermal annealing. The polymer melting behavior is mainly characterized by a shape transition from a straight to a curved line profile that fits well with the cubical function model used. This observation rather underlines the significance of using a nonlinear profile model in the VLAS instead of a rectangular or trapezoidal model which are unable to characterize such aspects of the polymer flow behavior.

As shown in Fig. 4(b), the short thermal annealing resulted in a large increase in the sidewall slope and decrease in the line height, but a somewhat weaker increase in the linewidth and the residual thickness. The curvatures shown in Fig. 4(b) look similar to the pronounced rippling pattern of the SU-8 structures in Fig. 3(b), indicating that the relaxation of the PMMA patterns is more significant at the high stress locations. If only the viscous flow is considered for the polymer relaxation, 950 000 PMMA nanostructures should maintain their morphology for a long period of time during the thermal annealing at its T_g due to their high viscosity at this temperature. However, the curved sidewalls quickly appear in the short annealing time (2–4 min). This fast shape evolution of the polymer structures is likely driven by the relaxation of stresses rather than the viscous flow. For the high molecular weight polymer, a high stress can be induced in the molecular entanglements during the nanoimprint process. In addition, a longer annealing time of 4 min was needed for the 2 μm pitch sample to exhibit similar profile changes compared to the 365 nm pitch sample. During thermal annealing, higher stress in the polymer structures should result in faster structural relaxation. Therefore, the faster relaxation during thermal annealing for the 365 nm pitch sample indicates the existence of higher stress in the PMMA gratings in comparison to the 2 μm pitch sample.

This experiment suggests that for better stability of polymer nanostructures formed by imprinting, the internal stress should be alleviated by optimizing polymer thickness, molecular weight, and imprint conditions.

IV. SUMMARY

A noninvasive and low cost visible light angular scatterometry technique is developed to precisely characterize the line profile geometry, dimensions, and residual thickness of the PMMA nanostructures made by nanoimprint lithography. This technique shows high accuracy in the measurements and the resolved profiles were in good agreement with the SEM images. This metrology was then used to study the effect of the polymer thickness on the flow behavior during nanoimprint, as well as the relaxation behavior of polymer nanostructures upon thermal annealing.

It is found in the experiments that the ratio of the mold dimensions to the polymer thickness strongly affects the

polymer flow behaviors and also the uniformity of residual thickness. A simple polymer flow model is presented to interpret the VLAS results and adds more insight to the residual thickness effects, flow dynamics, and stress buildup. Furthermore, polymer shape evolution during heating at its T_g is monitored using VLAS with a nonlinear sidewall profile model. This model is found accurate and suitable for observing increased curvature around the line bottom corners due to melting in the PMMA nanostructures. Similar curvatures were observed in imprinted SU-8 structures with a rippling pattern that visualizes the stress distribution in the polymer. This investigation reveals a strong dependence of polymer relaxation/stability behavior on the stress distribution in the polymer. The in-depth knowledge of the polymer flow behavior will be important for a better control of the nanoimprint process and high pattern transfer fidelity.

ACKNOWLEDGMENT

The authors thank Dale M. Byrne at the University of Texas at Dallas for his in-kind donation of the parts for scatterometry and for previous work on the equipment and also modeling algorithms. This work is supported in part by the Texas Higher Education Coordinating Board through Advanced Research Program under Contract No. 009741-0015-2006.

[1]S. Y. Chou, P. R. Krauss, W. Zhang, L. Guo, and L. Zhuang, J. Vac. Sci. Technol. B **15**, 2897 (1997).
[2]D. J. Resnick, S. V. Sreenivasan, and C. G. Willson, Mater. Today **8**, 34 (2005).
[3]F. Hua *et al.*, Nano Lett. **4**, 2467 (2004).
[4]M. D. Austin, H. X. Ge, W. Wu, M. T. Li, Z. N. Yu, D. Wasserman, S. A. Lyon, and S. Y. Chou, Appl. Phys. Lett. **84**, 5299 (2004).
[5]2006 International Technology Roadmap for Semiconductors (http://www.itrs.net/Links/2006Update/2006UpdateFinal.htm).
[6]S. S. H. Naqvi, J. R. McNeil, R. H. Krukar, and K. P. Bishop, Microlithogr. World **2**, 5 (1993).
[7]R. L. Jones, T. Hu, E. K. Lin, and W. Wu, Appl. Phys. Lett. **83**, 4059 (2003).
[8]R. Jones, T. J. Hu, C. L. Soles, E. K. Lin, W. Hu, R. M. Reano, S. W. Pang, and D. M. Casa, J. Microlithogr., Microfabr., Microsyst. **5**, 013001 (2006).
[9]H. Lee, H. W. Ro, C. L. Soles, R. L. Jones, E. K. Lin, W. Wu, and D. R. Hines, J. Vac. Sci. Technol. B **23**, 3023 (2005).
[10]R. L. Jones, T. Hu, C. L. Soles, E. K. Lin, R. M. Reano, S. W. Pang, and D. M. Casa, Nano Lett. **6**, 1723 (2004).
[11]D. Fuard, C. Perret, V. Farys, C. Gourgon, and P. Schiavone, J. Vac. Sci. Technol. B **23**, 3069 (2005).
[12]L. J. Heyderman, H. Schift, C. Davida, J. Gobrechta, and T. Schweizerb, Microelectron. Eng. **54**, 229 (2000).
[13]Y. Hirai, T. Konishi, T. Yoshikawa, and S. Yoshida, J. Vac. Sci. Technol. B **22**, 3288 (2004).
[14]H. D. Rowland, A. C. Sun, P. R. Schunk, and W. P. King, J. Micromech. Microeng. **15**, 2414 (2005).
[15]H.-C. Scheer, N. Bogdanski, M. Wissen, T. Konishib, and Y. Hirai, Microelectron. Eng. **83**, 843 (2006).
[16]R. M. Al-Assaad, L. Tao, and W. Hu, J. Microlithogr., Microfabr., Microsyst. (in press).
[17]E. M. Drege and D. M. Byrne, Proc. SPIE **3998**, 147 (2000).
[18]M. G. Moharam and T. K. Gaylord, J. Opt. Soc. Am. **71**, 811 (1981).
[19]S. Landis, N. Chaix, C. Gourgon, C. Perret, and T. Leveder, Nanotechnology **17**, 2701 (2006).
[20]V. Sirotkin, A. Svintsov, H. Schift, and S. Zaitsev, Microelectron. Eng. **84**, 868 (2007).